

# Emulation of MIMO Nonisotropic Fading Environments With Reverberation Chambers

Juan F. Valenzuela-Valdés, Antonio M. Martínez-González, and David A. Sánchez-Hernández, *Senior Member, IEEE*

**Abstract**—Some recent publications have extended the emulating capabilities of reverberation chambers. While polarization imbalance has been removed and Ricean-fading environments are now properly emulated, these chambers are still limited to isotropic nonline of sight (NLOS) scattering. By controlling the power received, number of resolvable multipath components (MPC), angular spread (AS), and angle of arrival (AoA), the emulation of real-propagating environments with both isotropic and nonisotropic scattering are demonstrated in this letter using a reverberation chamber with several multiple-input–multiple-output (MIMO) arrays.

**Index Terms**—K-factor, q-factor, reverberation chamber.

## I. INTRODUCTION

WIRELESS channel behaviour has received much attention in recent years, particularly multiple-input–multiple-output (MIMO) techniques as a way to increase the channel capacity. Channel modeling is normally divided into physical and not physical models. Two essential parameters of physical model are the number of scatters (NS), closely related to the number of resolvable multipath components (MPC), and the angular spread (AS). In fact, it has been demonstrated that MIMO capacity increases linearly with the AS for a linear array [1]. System performance also depends on angle of arrival (AoA) and angle of departure (AoD), which have been widely studied in the literature. Likewise, reverberation chambers are employed to emulate the wireless channel behavior in order to avoid long and cumbersome measurement campaigns. A reverberation chamber is typically a metallic enclosure wherein the electromagnetic field distribution is stirred by several means in order to obtain a field distribution that is statistically isotropic and homogeneous. The associated power density within the reverberation chamber typically follows that of an isotropic multipath environment [2]. The emulating possibilities of these chambers are typically limited to Rayleigh-fading scenarios with isotropic scattering, some elevation angles and restricted polarization diversity. Some recent papers have demonstrated the ability of reverberation chamber to emulate Ricean-fading

environments [3] and to eliminate typical polarization imbalance [4], and therefore reverberation chamber are acquiring wider acceptance as validating tools.

In this letter, we have demonstrated that it is also possible to emulate Rayleigh-fading scenarios with nonisotropic scattering using reverberation chambers. Seven different scenarios are employed with diverse AoA, AS, and MPC, and their associated correlation and cluster data properties are provided. Despite the need for further research to accurately characterize the novel emulation capabilities, the goal of this letter is to demonstrate that reverberation chambers can be used to emulate realistic propagation environments by providing some measured quantitative data.

## II. EMULATING AND MEASURING TECHNIQUES

The measurements were carried out in our indoor laboratory at the Technical University of Cartagena in Spain. The RC800 reverberation chamber by Bluetest AB was used in a corner of a  $4\text{ m} \times 5\text{ m} \times 3\text{ m}$  room. The RC800 has dimensions of  $0.8\text{ m} \times 1\text{ m} \times 1.6\text{ m}$ . Three wall-mounted antennas, three polarization stirring positions, one mechanical stirrer with 10 different positions, for each five different position of a second mechanical stirrer, a fixed platform position and 50-MHz frequency stirring were used. Measurements were performed at 1800 MHz and half-wave dipoles were used as MIMO array antennas.

Seven different measuring scenarios were prepared. Scenario A represents an empty reverberation chamber, providing the typical isotropic scattering. In Scenario B, one absorber piece of 24 cones is placed on the right-hand side wall of the chamber. Since the dipoles do not receive the expected multipath component of the absorbed side [5], a nonisotropic scattering scenario is obtained with modified AoA and reduced MPC compared to Scenario A. In Scenario C, two absorbers are used instead of one by adding a second absorber to the left-hand side, and a modified AoA histogram along with a further reduction of MPC is expected. Two and four PTFE 30-cm-high hollow cylinders of 5-cm-radius filled with lossy CENELEC Head Simulating Liquid (HSL) at the frequency of interest are introduced in the empty chamber to provide for Scenarios D and E, respectively. The filled cylinders make the Q-factor of the chamber decrease [3], slightly increasing the K-factor but a change in the AoA histogram and a further reduction in the MPC is also expected. The chamber door was left open in Scenario F, and the receiving antennas were located further apart outside the chamber just in front of the open door. In this way, nonisotropic scattering is again obtained, modifying AoA and MPC. Finally, Scenario G has the same configuration than Scenario F, but with the receiving antennas placed in the lateral side outside the chamber,

Manuscript received November 6, 2007; revised April 10, 2008. First published July 17, 2008. This work was supported in part by the Fundación Séneca, the R&D unit of the Autonomous Region of Murcia (Spain) under project references TIC-TEC 07/02-0005 and by the Spanish National R&D Programme through TEC2007/63470/TCM.

J. F. Valenzuela-Valdés is with the EMITE Ingeniería SLNE, E-30100 Espinardo, Murcia, Spain (e-mail: juan.valenzuela@emite-ingenieria.es).

A. M. Martínez-González and D. A. Sánchez-Hernández are with the Departamento de Tecnologías de la Información y Comunicaciones, Universidad Politécnica de Cartagena, Cartagena E-30202, Spain (e-mail: david.sanchez@upct.es).

Digital Object Identifier 10.1109/LAWP.2008.928488

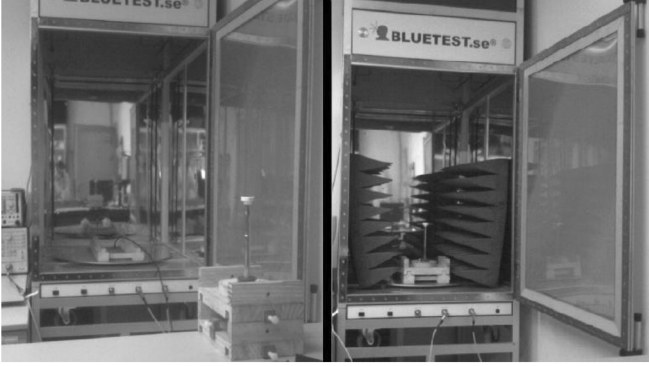


Fig. 1. Emulated fading scenarios with RC800. Left: Scenario C (door open for view only). Right: Scenario F.

TABLE I  
EVALUATED MIMO ARRAYS

	Spatial Diversity $D=d/\lambda$	Array size (TxR)
MIMO Array A.1	0.05	3x3
MIMO Array A.2	0.10	3x3
MIMO Array A.3	0.15	3x3
MIMO Array A.4	0.20	3x3
MIMO Array A.5	0.25	3x3
MIMO Array A.6	0.05	3x4
MIMO Array A.7	0.10	3x4
MIMO Array A.8	0.15	3x4

providing a further modification of AoA, AS, and MPC compared to Scenario F. Since no absorbers or cylinders are employed, an increment on the AS is expected for Scenarios F and G in comparison to the others.

A photograph of some of these scenarios (C and F) is depicted in Fig. 1. Likewise, in order to evaluate the correlation and cluster data properties in all these measuring scenarios, eight different MIMO arrays were employed using spatial-diversity for each of the measuring scenarios. The employed  $T \times R$  MIMO arrays are listed in Table I for Scenario A as an example, where  $d$  is the interelement spacing  $D = d/\lambda$ , and  $T$  and  $R$  indicate the number of transmitting and receiving antennas, respectively.

### III. EVALUATION METHODS

The K-factor of the employed scenarios has been evaluated by an estimation of the Q-factor using the cavity theory and by experimental data analyses.

#### A. Estimation of the Q-Factor

The Q-factor of a cavity can be estimated from the average power transmission level  $P$  by [6]

$$Q = 16 * \pi^2 * V * c^{-3} * f^3 * P \quad (1)$$

where  $V$  is the volume of the cavity,  $c$  is the speed of light, and  $f$  is the frequency of operation. The K-factor can be calculated from the Q-factor by [3]

$$K = \frac{3 * V * D}{2 * \lambda * Q * d^2} \quad (2)$$

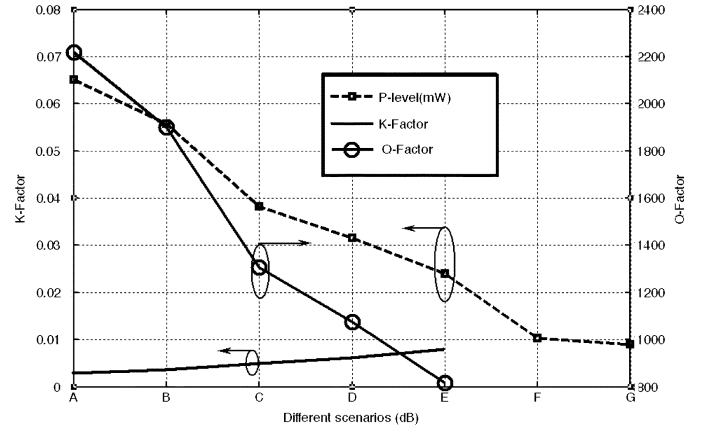


Fig. 2. Evaluation of received power level, K-factor, and Q-factor for all scenarios.

where  $D$  is the directivity of the antenna under test,  $\lambda$  is the wavelength, and  $d$  is distance between antennas. By combining (1) and (2) we obtain

$$K = \frac{3 * D * \lambda^2}{32 * \pi^2 * P * d^2} \quad (3)$$

The received power, Q-factor and K-factor evaluated using this method for all scenarios are plotted in Fig. 2. As it was expected, the power level decreases with increasing volume of lossy material. The Q-factor decreases progressively in Scenarios B to E respect to Scenario A due to the lossy material that was introduced inside the chamber. When the door is open and the number of modes consequently increased (Scenarios F and G), the situation can no longer be considered that of a cavity, and no Q-factor or associated K-factor is depicted. The values of the K-factor are very low, always below 0.02, thus, providing a Rayleigh-fading-like environment for all emulated scenarios.

#### B. Experimental Data Analyses

The K-factor can also be calculated from measured S-parameter in a reverberation chamber by [3]

$$K = \frac{d_R^2}{2\sigma_R^2} = \frac{(|\langle s_{21} \rangle|)^2}{\langle |s_{21} - \langle s_{21} \rangle|^2 \rangle} \quad (4)$$

where  $S_{21}$  is the measured parameter in the reverberation chamber for each antenna pair,  $\sigma_R$  is the radius of cluster data, and  $d_R$  is the distance of centroid of cluster from the origin. As an example, the scatter plots [3] of measured  $S_{21}$  between the  $T_1 - R_1$  antenna pairs and  $\sigma_R$  for all scenarios are depicted in Figs. 3 and 4, respectively. In these figures, the  $x$  and  $y$  axis represent the real and imaginary part of  $S_{21}$ , respectively. A scatter plot would result in the data clustered in a circle and centered about the origin for pure Rayleigh-fading environments. As the direct line of sight (LoS) energy became comparable to the non-LoS energy, the cluster of data would move away from the origin, and the fading environment becomes a Rician one. Scatter plots are useful not only for identifying the LoS behavior of the fading environments, but also to quantify the data dispersion through the K-factor. It can be observed from Figs. 3 and 4 that  $\sigma_R$  decreases with increasing load of the chamber. Finally, the averaged K-factor obtained from data analyses of

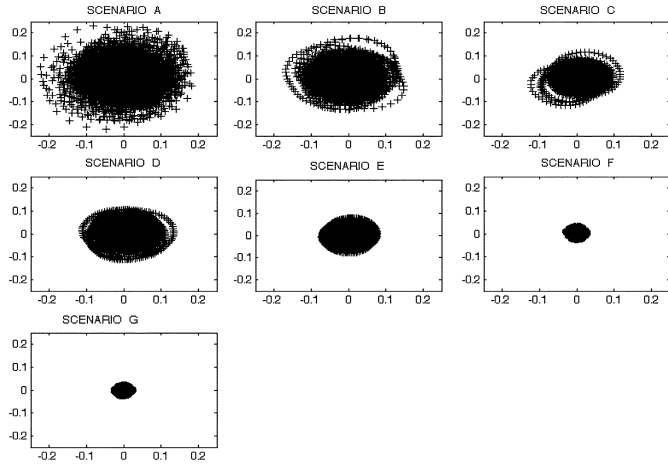
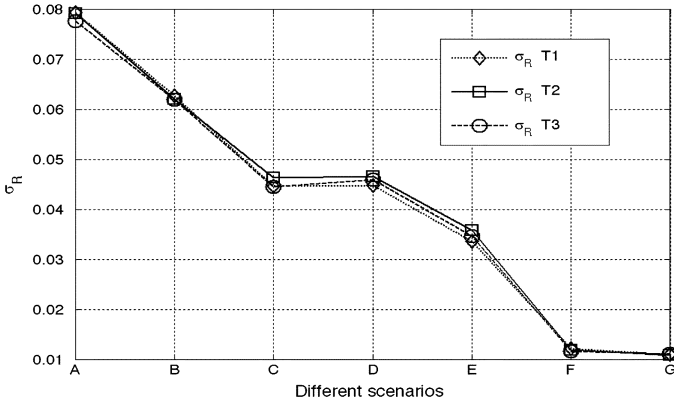


Fig. 3. Scatter plots for all emulated scenarios.


 Fig. 4.  $\sigma_R$  for all scenarios and transmitter antennas.

the performed measurements taken is shown in Fig. 5, along with a comparison to K-factors estimated from the Q-factors. From this figure, one can observe that the two methods used for estimating the K-factor tend to provide similar results for all scenarios except for those wherein the chamber door is open (F and G), where the cavity method cannot be applied. Reducing the Q-factor of the chamber with absorbing material (Scenarios B to E) did not change the size of the cavity, and consequently the estimating method based on the Q-factor provided good results. When the door was open, however, the measured scenario could no longer be represented by a cavity, and a proper estimation of the K-factor was only obtained from the data taken from measurements.

#### IV. MEASURED RESULTS

The correlation function in a MIMO system depends strongly on the multipath parameters such as AS, MPC, or AoA [7], [8]. The measured correlation coefficient between any two antennas in the array for all emulated scenarios and arrays is illustrated in Fig. 6.

The results depicted in Fig. 6 show an increasing correlation coefficient with decreasing MPC (NS), which has also been previously reported [9]. As expected, the lowest correlation coefficient is obtained for Scenario A, i.e., for isotropic scattering. In Scenario F, the correlation is found to be similar to Scenarios

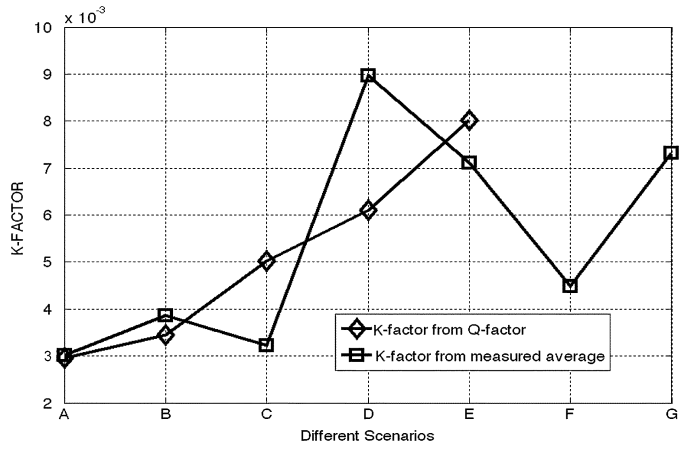


Fig. 5. K-factors for all scenarios.

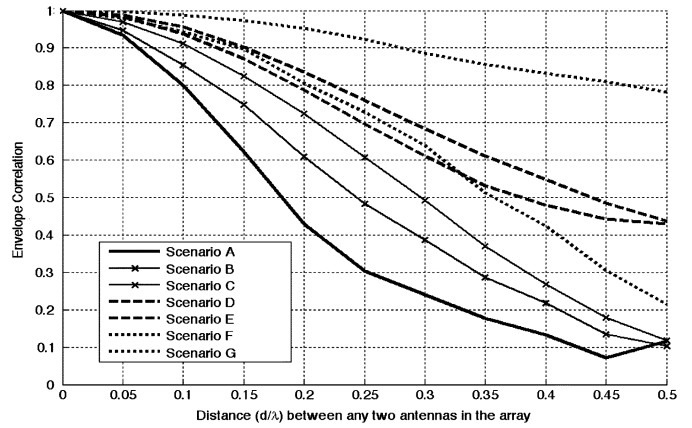


Fig. 6. Correlation coefficients for all scenarios.

D and E until  $D = (d/\lambda) = 0.35$ . While the higher correlation in Scenarios B and C respect to Scenario A is due to the use of absorbers, for Scenarios D and E, this is due to the presence of the HSL-full cylinders. Scenarios F and G are also highly correlated despite the larger distance between transmit and receive antennas. This is due to a considerable reduction in the MPC when the door is open. Consequently, a decrease in capacity is expected for Scenarios F and G. In order to provide quantitative data and to confirm the described relationship between correlation and multipath parameters, the number of resolvable MPC, AS, and AoA histograms were measured for all scenarios.

In Fig. 7, the measured eigenvalues of the data matrix for all scenarios are depicted. In this figure, the number of MPC was determined from the relative decrease between neighboring eigenvalues and confirmed by visual inspection of plots. For each MPC, the transfer function between all pairs of antennas were estimated by multiple signal classification (MUSIC) high-resolution algorithm [10] with pseudoinverse. The number of resolvable MPC ranged from 12 to 24, and decreases with ascending scenario letter (A to G), as expected. The decrease in MPC for the scenarios with the open door (F and G) and no absorbers or cylinders, however, would result in an increment of AS. This is confirmed by Fig. 8, wherein the AoA is calculated from the measured data again using the MUSIC high resolution algorithm [10]. The algorithm was modified to account for the

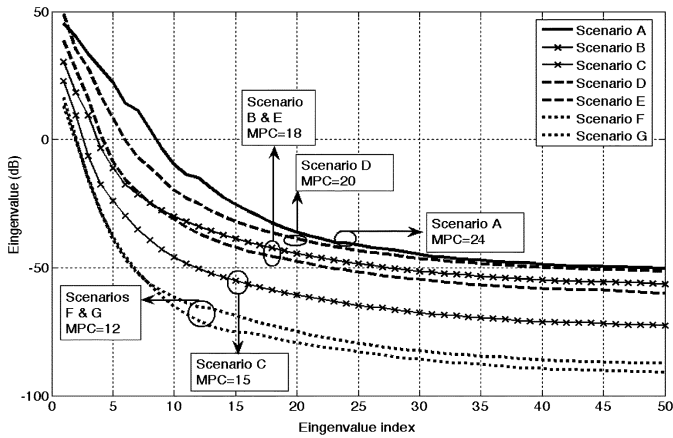


Fig. 7. Measured eigenvalues of the data matrix for all scenarios.

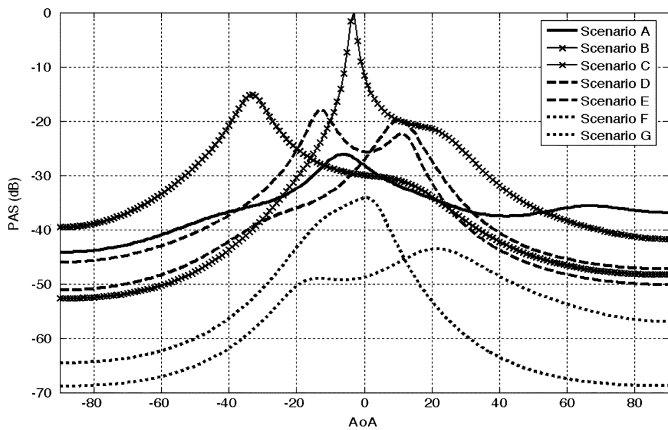


Fig. 8. Histograms of measured AoA using the high resolution MUSIC algorithm.

fact that our receiving antennas are dipoles and therefore the radiation patterns are not constant as a function of the incident angle.

Fig. 8 clearly shows the effect of the diverse scenarios on the AoA. The conventional enclosed chamber operation (Scenario A) shows a quasi-uniform angle distribution of energy, with power differences around 20 dB for diverse angles. This confirms the quasi-isotropic behavior of the chamber, where the isotropicity could be improved by using more stirred positions. The addition of one absorber (Scenario B) displaces the AoA to the chamber side where there is no absorber, while adding two symmetric absorbers (Scenario C) makes a narrower AS, as expected. The use of liquid-filled cylinders in Scenarios D and E at close presence of the antennas grants a different situation. The cylinders have to absorb energy, but due to the large difference between the HSL permittivity and the air they also scatter a large amount of the incident power. This can be observed in Fig. 8 for Scenario D, where the AoA is displaced to the side where the pair of cylinders is located, and for Scenario E, where

two different clusters are identified in the azimuth directions where the two pairs of cylinders are located. From Fig. 7, one can also see that these scatters become relevant ones instead of existing ones, and MPC is not increased. Finally, Scenarios F and G (door open), confirm the expected increase in the AS, as well as the decrease in the received power due to the larger separation between the transmit and receive arrays. Measured AS values defined as in [1] were 0.21, 0.18, 0.09, 0.20, 0.18, 0.23, and 0.27 for Scenarios A to G, respectively. In all modified scenarios, a nonisotropic behavior is observed, with up to 50-dB power differences for diverse angles.

## V. CONCLUSION

Diverse nonisotropic Rayleigh-fading environments have been emulated with a reverberation chamber. Different cluster data, correlation properties and multipath parameters have been obtained for diverse MIMO arrays. Despite the low K-factors obtained with the chamber, the differences in AoA, NS, and AS provided different correlation properties. In addition, we have shown that when the chamber door is open, an estimation of the emulated K-factor can only be ensured by processing the measured data. Accurate characterization of the new environments been emulated is foreseen, particularly for the sensitivity to deviations effects in the time domain.

## REFERENCES

- [1] A. S. Y. Poon, D. N. C. Tse, and R. W. Brodersen, "Impact of scattering on the capacity, diversity, and propagation range of multiple-antenna channels," *IEEE Trans. Inf. Theory*, vol. 52, no. 3, pp. 1087–1100, Mar. 2006.
- [2] K. Rosengren and P.-S. Kildal, "Theoretical study of angular distribution of plane waves in a small reverberation chamber for simulating multipath environment and testing mobile phones," in *Proc. IEEE Antennas Propag. Soc. Int. Symp.*, 2001, vol. 3, pp. 358–361, vol. 3.
- [3] C. L. Holloway, D. A. Hill, J. M. Ladbury, P. F. Wilson, G. Koepke, and J. Coder, "On the use of reverberation chambers to simulate a rician radio environment for the testing of wireless devices," *IEEE Trans. Antennas Propag.*, vol. 54, no. 11, pp. 3167–3177, Nov. 2006.
- [4] P. S. Kildal and C. Carlsson, "Detection of a polarization imbalance in reverberation chambers and how to remove it by polarization stirring when measuring antenna efficiencies," *Microw. Opt. Technol. Lett.*, vol. 34, no. 2, pp. 145–149, Jul. 2002.
- [5] M. Otterskog and K. Madsen, "On creating a non-isotropic propagation environment inside a scattered field chamber," *Microw. Opt. Technol. Lett.*, vol. 43, no. 3, pp. 192–195, Nov. 2005.
- [6] D. A. Hill, M. T. Ma, A. R. Ondrejka, B. F. Riddle, M. L. Crawford, and R. T. Johnk, "Aperture excitation of electrically large, Lossy cavities," *IEEE Trans. Electromagn. Compat.*, vol. 3, no. 3, pp. 169–178, Aug. 1994.
- [7] P. D. Teal, T. D. Abahayapala, and R. A. Kennedy, "Spatial correlation for general distributions of scatterers," *IEEE Signal Process. Lett.*, vol. 9, no. 10, pp. 305–308, Oct. 2002.
- [8] K. Anim-Appiah, "Complex envelope correlations for non-isotropic scattering," *Electron. Lett.*, vol. 34, no. 9, pp. 918–919, Apr. 1998.
- [9] Z. Tang and A. S. Mohan, "Characterize the indoor multipath propagation for MIMO communications," in *Proc. Asia-Pacific Microw. Conf. (APMC)*, Dec. 2005, vol. 4, p. 4.
- [10] H. S. Rad and S. Gazor, "A 3D correlation model for MIMO non-isotropic scattering with arbitrary antenna arrays," in *Proc. IEEE Wireless Commun. Netw. Conf.*, Mar. 2005, vol. 2, pp. 938–943.